HHS Public Access

Author manuscript

Biotechnol Bioeng. Author manuscript; available in PMC 2021 February 01.

Published in final edited form as:

Biotechnol Bioeng. 2020 February ; 117(2): 486–497. doi:10.1002/bit.27188.

Multi-organ Microfluidic Platform with Breathable Lung Chamber for Inhalation or Intravenous Drug Screening and Development

Paula G. Miller[1,2], **Chen-Yu Chen**[1], **Ying I. Wang**[1], **Emily Gao**[1,2], **Michael L. Shuler**[1,2]

[1]Nancy E. and Peter C. Meinig School of Biomedical Engineering, Cornell University, Ithaca, NY 14853, USA.

[2]Robert Frederick Smith School of Chemical and Biomolecular Engineering, Cornell University, Ithaca, NY 14853, USA

Abstract

Efficient and economical delivery of pharmaceuticals to patients is critical for effective therapy. Here we describe a multiorgan (lung, liver and breast cancer) microphysiological system ("Body-on-a-Chip") designed to mimic both inhalation therapy and/or intravenous therapy using curcumin as a model drug. This system is "pumpless" and self-contained using a rocker platform for fluid (blood surrogate) bidirectional recirculation. Our lung chamber is constructed to maintain an air-liquid interface and contained a "breathable" component that was designed to mimic breathing by simulating gas exchange, contraction and expansion of the "lung" using a reciprocating pump. Three cell lines were used: A549 for the lung, HepG2 C3A for the liver, and MDA MB231 for breast cancer. All cell lines were maintained with high viability (>85%) in the device for at least 48 hours. Curcumin is used to treat breast cancer and this allowed us to compare inhalation delivery versus intravenous delivery of the drug in terms of effectiveness and potentially toxicity. Inhalation therapy could be potentially applied at home by the patient while intravenous therapy would need to be applied in a clinical setting. Inhalation therapy would be more economical and allow more frequent dosing with a potentially lower level of drug. For 24 hour exposure to 2.5 and 25 μM curcumin in the flow device the effect on lung and liver viability was small to insignificant, while there was a significant decrease in viability of the breast cancer (to 69% at 2.5 μM and 51% at 25 μM). Intravenous delivery also selectively decreased breast cancer viability (to 88% at 2.5 μM and 79% at 25 μM) but was less effective than inhalation therapy. The response in the static device controls was significantly reduced from that with recirculation demonstrating the effect of flow. These results demonstrate for the first time the feasibility of constructing a multiorgan microphysiological system with recirculating flow that incorporates a "breathable" lung module that maintains an air-liquid interface.

Keywords

multiorgan physiologic system; breathable lung module; inhalation and intravenous drug delivery

Corresponding author: Paula Miller, Address: 379 Kimball Hall, Biomedical Engineering,Cornell University, Ithaca, New York 14853-7202, Phone: 607 255-5204, pgm6@cornell.edu.

Introduction

Inhalation drug delivery is a promising approach to treating for both pulmonary and systemic illnesses due to its non-invasive nature and reproducible absorption kinetics (Labiris et al., 2003). Inhalation therapy is a common treatment for patients with asthma and chronic obstructive pulmonary diseases (COPD). For asthma, beta-2-agonist treatment is often applied, as it helps with the relaxation of mouth muscles. However, it triggers severe side-effects if taken orally, but a reduced level of side-effects is present when inhaled. Another positive property of inhalation therapy for lung diseases is that inhalation delivers the drug directly to the desired site, the lungs. It is a rapid and effective pharmacodynamic approach for drug administration to the lungs with less drug accumulation in nontargeted body parts. Due to its high level of drug safety, inhalation administration has become the most common treatment for long-term COPD or asthma treatment (Billington et al., 2017). While the focus has been on treating lung disease there is a direct exchange between the alveoli and the blood so drugs may enter the systemic system and potentially treat systemic disease (Labiris et al., 2003).

Estimating human response to inhalation drugs often face obstacles in the screening process due to time, cost and the process generally requires animal studies. Unfortunately, animal studies are often not an accurate representation of the human body and raise ethical concerns (Driscoll et al., 2000). Parameters, such as, lung size, volume, elasticity, dynamic resistance and respiratory flow have been reported to be different between human and animal models (Irvin et al., 2003) (Tu et al., 1995) (Persson, 2002). Although animal models are limited in predicting the complex human physiology, they can serve to provide *in vivo* information (Mak et al., 2014).

An alternative to animal studies are *in vitro* systems using human cell cultures or constructs. Normally these *in vitro* studies rely on static cultures, such as multi-well plates. However, these systems cannot recreate the cell to cell and organ to organ interactions that occur in the human body and do not mimic the dynamics of drug delivery such as intravenous and inhalation.

Microfluidic organ-on-a-chip systems have been introduced to replicate some of the cellular and organ to organ interactions that can occur when a body is exposed to pharmaceuticals (Esch et al., 2011; Wang et al., 2018; Wang et al., 2017). These devices can be modified to contain a breathable lung device to study lung physiology, disease, drug therapy and potentially inhalation drug therapy. Many single organ lung-on-a-chip models have been developed (e.g., Konar et al., 2016; Long et al., 2012; Douville NJ et al., 2011). Some researchers choose to focus on the branched structure to model the bronchi and alveoli, the capillary-lung cell interactions using lung organoids, the particle transport through the membrane, use of a small airway to mimic asthmatic crisis or use suspended gels to study epithelial and smooth muscle cell interactions (e.g., Los Alamos National Laboratory, 2016; Nikolic and Rawlins, 2017; Portkay et al., 2014; Benam et al., 2016; Humayun et al., 2018). A biomimetic microsystem was developed by the Ingber group that captures the functional alveolar-capillary interface and recreated a physiological breathing movement by applying a vacuum to the side chambers causing stretching (Huh et al., 2010 and Huh, 2015). This

group also used a human lung-on-a-chip device to study human pulmonary edema *in vitro* predicting potential drug efficacy in humans and to study intravascular thrombosis using primary human alveolar cells (Huh et al., 2012; Jain et al., 2018). A lung-on-a-chip array using a micro-diaphragm to stretch the alveolar barrier was developed to create robust reproducible devices and included the use of primary lung cells (Stucki et al., 2015; Stucki et al., 2018).

Here, we describe the design and operation of an *in vitro* device to provide a more effective way to screen drugs for inhalation as well as intravenous or oral administration and determine if inhalation therapy could possibly be used to treat systemic disease. Our lung module was designed to screen drugs for intravenous and/or inhalation therapy using human cell lines although it could use more sophisticated tissue constructs. This device was created to model physiologically relevant organ-to-organ and drug interactions *in vitro* through a PBPK model-based design. Our device aims to mimic the breathing mechanisms of the lung using a vacuum chamber, create a lung air-liquid interface that has been found to be important for normal lung airway biology (Pezzulo et al., 2011), and contain channels that connect the lung compartment with liver and tumor compartments. We use the term “compartment” to refer to the liquid and cellular components.

To model the air-liquid interface (ALI) found in the lung, past studies have used transwells in multiwell plates (Nalayanda et al., 2009). By modifying these procedures, we designed an “ALI bridge” to support our lung membranes and create the air-liquid interface to be inserted into our breathable lung device. This “ALI bridge” design allowed direct visual observation of the lung membrane so we could observe the air-liquid interface before it was inserted into our complete lung chamber. The term “complete lung chamber” refers to the combination of the vacuum chamber (where vacuum is applied) (breathable component), the air-liquid interface, lung cellular membrane and medium (lung compartment).

Then we also modified the hanging drop method to introduce HepG2 C3A liver cells and MDA MB231 breast cells onto a scaffold (Foty et al., 2011). We used hanging drops to improve the cellular coverage of scaffolds and create 3 dimensional-like (3D) structures which tend to be more representative of the tumor physiology. This technique was particularly useful in creating the 3D constructs we desired for the breathable lung device for testing inhalation and intravenous drug therapies.

Here, we used a microphysiological system (aka “Body-on-a-Chip”) to demonstrate for the first time integration of a “breathable” lung module able to maintain a stable air-liquid interface with systemic circulation including two other tissue modules (liver and breast cancer). The resulting device was challenged with curcumin (a chemotherapeutic drug used to treat a breast cancer module) and we compared the intravenous and inhalation drug delivery cytotoxic effects.

Materials and Methods

Cell Cultures and Chemicals

The A549 and HepG2 C3A cell lines were obtained from the American Type Culture Collection (ATCC) (Manassas, VA) and MDA MB231 was a generous gift from Dr. Claudia Fischbach's laboratory (Cornell University). These cells were maintained in Eagle's Minimum Essential Medium (EMEM) plus 10% fetal bovine serum (Lonza #12–611F, Invitrogen #26140079) (Allendale, NJ; Carlsbad, CA) in a humidified incubator, at 37°C and 5% CO_2. The confluent cell cultures were washed with Dulbecco's Phosphate Buffered Saline (DPBS)(Invitrogen), detached using 0.25% trypsin – 0.53 mM EDTA solution (Invitrogen #25200), subcultured in culture flasks and plated on membranes or scaffolds to be used in devices or for static controls.

The common circulating medium used for static and device experiments was EMEM plus 10% Fetal Bovine Serum and is referred to as "device medium".

Overall Device Design

We designed a microphysiological device (Figure 1A, B) consisting of a poly(methyl methacrylate (PMMA) frame (5.5 mm thick) (McMaster Carr #8560K179, Cleveland, OH), two layers of clear silicone gaskets (0.5 mm thick and 0.25 mm thick)(Sigma #GBL664571, GBL664475, St. Louis, MO) and a polycarbonate porous nucleopore track-etched membrane (0.4 μm pore size)(Whatman #111707, Clifton, NJ), 2 connectors (McMaster Carr #534115K289), 6 18–8 stainless steel flanged screw-to-expand inserts (McMaster Carr #95110A110), and 6 18–8 stainless steel pan head Phillips screws (McMaster Carr #91772A059). The PMMA frame (PMMA lid and PMMA base with channels, compartments and reservoirs) and silicone gaskets were designed in Corel Draw (Corel Corporation, Ottawa, Ontario) and were cut/etched with the VersaLaser VLS3.60 Cutting and Engraving CO_2 Laser (Universal Laser Systems, Scottsdale, Arizona) to create reservoirs, compartments and channels (Figure 1A – D).

Cellular Compartments

The volumes of the liver and lung for this device were scaled down proportionately from the average human male organ volumes reported by Price and Haber by a factor of 33,400 (Haber et al., 2013, Price et al., 2003). The tumor volume was set to a volume that was comfortable to pipet (3 μL) and the other organs were scaled accordingly. In this lung design, we had three parallel channels that provided medium to each target organ/compartment. The lung cellular compartment held 47.1 μL, the liver cellular compartment held 30.3 μL and the tumor cellular compartment held 3 μL cells and medium.

Complete Lung Chamber

The goal of our lung chamber was to create a breathable lung model. (1) The chamber provided the lung cells with medium on one side of the gasket layer (liquid interface) and direct air exposure to the cells on the other side (air interface) with the capability of expanding/contracting (breathable component) (Figure 1A, B). (2) Liquid Interface was created by etching a lung cellular compartment into the bottom frame of the device, filling it

with device medium, and layering a lung membrane layer on top. The lung membrane layer was created by plating lung cells onto a polycarbonate porous nucleopore track-etch membrane (0.4 μm pore size) that was sandwiched between two laser cut silicone layers (0.5 mm thick). The lung cells sat above the lung compartment being fed from below through the membrane (liquid interface) and the other side of the cells were exposed to the atmosphere (air interface). (3) The PMMA lid of the device was cut to provide two open wells/inlets for the lung chamber, one provided direct access to the lung cells via the air inlet and the other inlet created the breathable portion by connecting the vacuum chamber to the reciprocating pump (Figure 1B). (4) Specifically, the breathable component was created by attaching a flexible silicone expansion layer (0.25 mm thick) to the inside of the top lid with a thin layer of an epoxy mixture (LOCTITE Quick-set) (where vacuum could be applied and released), after assembly two lengths of tubing with a 0.2 μm syringe filter in-between were connected to the vacuum pump adaptor (breathable port on top PMMA lid) and the reciprocating syringe pump (developed by Lincoln Young, INEng, LLC, Ithaca, New York). The vacuum/release movement of the pump on the expansion layer was tested to ensure that we could obtain a breathable component (Figure 2).

The epoxy provided a secure hold and no epoxy was exposed to the medium after assembly so cytotoxicity was not an issue. A similar finding was also reported in a study of the cytotoxicity of an epoxy coating on human fibroblasts (Ragonha et al., 2015).

Liver and Tumor Compartments

The liver and tumor compartments were etched into the PMMA base. 3D scaffolds (cut from Lena Bioscience SeedEZ cell culture sheets (Sigma #Z742249)) with attached cells were placed into the liver or tumor compartments. The scaffold from Lena Biosciences SeedEZ™ 3D Cell Culture System was chosen because of its adaptability to different situations and its ability to be autoclaved. Figure 1A and B shows a schematic of the layers integrated in this device and a cross-section of the complete lung chamber. Figure 1C and D shows a photograph of the frame of the actual device and how the silicone layers were cut with the VersaLaser.

Channel Calculations

The channels to feed the chambers were etched in the PMMA base by using Corel Draw to design and the VersaLaser to raster cut. We used the following formulas to determine the desired channel dimensions needed to provide flow rates that were close to the scaled physiological rates (based on reported values for an average human male (Haber et al., 2013; Price et al., 2003):

Residence Time=Organ volume/Flow rate

$$T = V/Q \quad (1)$$

where T is the residence time (s), V is the organ volume (m^3) and Q is the flow rate ($m^3 s^{-1}$).

$$Q = \left(\frac{\rho g \pi}{8\eta}\right) \times \left(\frac{\Delta h (R_H)^4}{L}\right) \quad (2)$$

where Q = volumetric flow rate ($m^3 s^{-1}$); ρ = density of the medium (kg m^{-3}); g = gravitational constant (9.8 m s^{-2}); Δh = height difference (L*sin [the angle of the rocker]), (m); R_H – hydraulic radius of the channel (m); η = fluid viscosity (Pa s); L = length of the channel (m). (Morier et al., 2004)

The hydraulic radius was calculated using equation (2) and then used to calculate the corresponding channel surface area, SA.

$$SA = \pi (R_H)^2 \quad (3)$$

The channels' (of our device) cross-sectional area was rectangular because the channels were etched with the VeraLaser. The formula for SA was designed for a circular cross-section but we were able to use this area to estimate the height and width of our channels. Table 1 provides physiological information and calculations used to create the lung device (Haber et al., 2013, Price et al., 2003).

The fluid flow in the overall device was driven by using a custom designed rocking program on an Infinity Rocker Platform (NextAdvance #IR103 with customized programs). Recirculation of the cell culture medium was achieved by a gravity-induced bidirectional flow (Sung et al., 2010; Miller and Shuler, 2016). The program used for these experiments was 60 s with each side in the highest position, with a 1 s flip in between and repeat. The observed flow rates were determined by screen capturing the videos of the flow of 0.4% trypan blue through the channels. Screenpresso (www.screenpresso.com) was used to capture the photographs and ImageJ (rsb.info.nih.gov/ij/download.html) was used to measure the distance the dye traveled down the channel. Microsoft Office Excel 2007 (www.microsoft.com) was used to calculate the average flow rates. The observed flow rates were within 8% of the desired flow rates, data not shown.

Cellular Preparation for Device Experiments

The lung cellular gasket layers (polycarbonate porous nucleopore track-etched membrane sandwiched between 2 silicone gaskets) were pre-assembled and autoclaved on a Kimwipes in a 100 mm glass petri dishes. The membranes were coated with collagen type I (100 μL of a 3 mg/mL concentration) (Gibco #A10483–01, Grand Island, NY) in sterile 100 mm dishes for 1 hour. A549 cells were dissociated and resuspended at a concentration of 5×10^{-4} cells/mL in device medium and 30.3 μL was plated onto these membranes. These cells were allowed to incubate for 2 hours in a humidified incubator, at 37°C and 5% CO_2, then more medium (10mL) was added and the membranes were returned to the incubator (day 0). On day 3, an air-interface was established. First, an air-interface bridge was autoclaved in a 150 mm dish. The air-interface bridge (bridge) was created by using 4 microscope slides, a strip from a 1.6 mm silicone sheet (Sigma #GBL664273), and clear silicone sealant (LOCTITE, Germany) in a 150 mm glass petri dish (Figure 3A). Briefly, 2 microscope slides were

attached to each other with the silicone sealant (2 sets), these 2 stacks were spaced 6 mm apart and the attached to each other with a silicone strip. The lung gaskets with cells (2 per bridge) were placed on top of the bridge and 20 mL of device medium was added below the bridge, every other day 50% of the medium was exchanged for fresh medium until device assembly on day 10. At the end of the 10-day period, a set of the A549 cells were saved for immunostaining to test for the presence of tight junctions (Figure 3B) (see below for procedures). It would have been nice to measure transeptihelial electrical resistance (TEER) to characterize the A549 barrier however it was not physically possible because of the design of the lung membrane layer.

The liver and tumor compartments contained 3 dimensional (3D) scaffold cellular constructs that were created using a modified hanging drop method (Foty, 2011). On day 7, cells (MDA-MB231, HepG2 C3A) were dissociated independently and resuspended to a concentration of 5×10^{-6} cells/mL. Five 3 μL drops of MDA-MB231 were plated on autoclaved 2 mm diameter scaffolds that were precut with a biopsy punch from Lena Bioscience SeedEZ cell culture sheet (Sigma #Z742249). Five 47.1 μL size drops of HepG2 C3A were plated on autoclaved 6 mm diameter scaffolds precut from a SeedEZ cell culture sheet. These scaffolds were placed separately onto a 2 μL drop on the inside of the top of 35 mm petri dishes, 2 mL of Dulbecco's Phosphate Buffered Saline was placed in the bottom of these dishes and the tops were flipped over to close the dishes. The cells were allowed to incubate in the humidified incubator for 2 hours, then the scaffolds with the attached cells were picked up with sterile forceps, place into separate 60 mm dishes with 5 mL fresh medium and incubated until assembly on day 10.

Device Preparation and Assembly

Most of the device parts were placed in 150 mm glass petri dishes and autoclaved. Kimwipes were placed in the bottom of the dishes to prevent the pre-assembled silicone layers from sticking to the bottom of the dishes during autoclaving. On day 10, the PMMA frame (not autoclavable) was soaked three times in penicillin/streptomycin (100 U mL^{-1}; 100 μg mL^{-1}) (Invitrogen #15140–122) for 30 min each and rinsed in DPBS (Invitrogen #14190) before assembly to prevent contamination and provide wetting of the channels. All components of the device were handled or manipulated with sterile forceps. To assemble the device, the PMMA base was placed into a sterile dish. Then, the MDA MB231 and HepG2 C3A scaffolds were place into their compartments. Device medium was added and then the lung gasket was carefully placed on top of the chambers containing scaffolds making sure the lung cellular region aligned with the lung compartment. Is was very important to avoid creating bubbles. Medium was **NOT** placed on top of the lung cells because we wanted to maintain the pre-created air-interface. Pre-autoclaved silicone tubing with a 0.2 μm syringe filter was connected to the vacuum chamber adaptor on the top of the PMMA lid, the lid was placed on the lung gasket and the device was secured with stainless steel screws. Then the device was placed into a pre-sterilized secondary container (pipet tip box (118 mm × 95 mm × 102 mm) with side slits that accommodated the exiting of silicone tubing, device medium was added to the reservoirs (1000 μL total volume in each device) and an extra sterile 35 mm dish (bottom only) of 5 mL DPBS was placed inside the sterile container to minimize evaporation from the small amount of liquid in the device. After closing the container, the

syringe filter end of the silicone tubing was attached to the other silicone tubing and connected to the reciprocating syringe pump (Figure 2). The reciprocating pump was kept outside of the incubator due to space restraints within the incubator. The fixed rate of the reciprocating pump was 5 complete cycles/minute. A cycle includes one complete expansion of the membrane (inhale) and one complete applied vacuum (exhale). The average normal respiratory rate for a healthy adult male is between 12 and 18 breaths per minute. Our reciprocating pump could only handle 5 breaths per minute because it was not a variable pump. Then the device within the sterile box was placed on the Infinity Rocker Platform. The program used for these experiments was 60 s with each side in the highest position, with a 1 s flip in between and repeat.

On day 10 the devices were assembled or static controls were set up and the experiments started (n = 3).

Toxicity Experiments

Preliminary static toxicity experiments were done using MDA MB231. Cells were detached, resuspended to obtain 5×10^{-4} cells/mL, 1 mL of the suspension was plated into eight 6-well-plates and incubated in the humidified incubator at 37°C and 5% CO_2. After 24 hours, the plates were divided into groups (6 wells per group per experiment) (n = 3 separate experiments) as follows: (a) Control (b) 1 μM curcumin (c) 10 μM curcumin (d) 20 μM curcumin (e.) 30 μM curcumin (f) 40 μM curcumin (g) 50 μM curcumin (1ml final volume). After 24 hours, 3 wells per group were washed, trypsinized with 0.25% trypsin-EDTA (500 μL), and neutralized (500 μL). 0.4% trypan blue was added and the viable cells were counted with a hemocytometer. ID_{50} values were calculated. After 72 hours, 3 wells per group were assessed in the same manner as the 24 hour group and the ID_{50} values calculated. After calculating our ID_{50} values (24 hour exposure = 22 μM and 72 hour exposure = 15 μM), we decided to use 2.5 μM and 25 μM curcumin as the concentrations of interest in the devices for 24 hour exposure. (Figure 4)

Toxicity screening was done at 24 hours in the microfluidic lung device and a static control system to determine if the delivery method (via reservoir (intravenous) vs. via lung (inhalation)) would make a difference in the toxic effect of curcumin on MDA MB231. On day 0, we plated A549 (lung) cells and let them grow for 3 days. On day 3, we set up the air-interface and we fed these cells with fresh medium from below the membrane on day 5 and day 7. On day 7, we plated HepG2 C3A (liver) cells and MDA MB231 (breast) cells onto scaffolds through the modified hanging drop method (see above), transferred them into dishes and allowed them to grow until day 10. See Chambers and Channel Calculations section for specific details about the device. On day 10, the devices were assembled (see Device Preparation and Assembly) and placed into the humidified incubator, at 37°C and 5% CO_2 for 24 hours. On day 11, medium samples for urea and albumin were collected and frozen at −80°C. Working stock solutions (2.5 mM and 0.25 mM) of curcumin (Sigma #C1386) were made fresh. The devices were divided into the following 24 hour exposure groups: (1) Control (2) 2.5 μM curcumin - reservoir (3) 25 μM curcumin - reservoir (4) 2.5 μM curcumin - lung chamber (5) 25 μM curcumin - lung chamber. First, a 50% fresh medium exchange (1000 μL final volume) was made in all the devices. Then the 2.5 μM

curcumin groups received 10 μL of a the 0.25 mM stock, the 25 μM curcumin groups received 10 μL of the 2.5 mM stock and the control groups received 10 μL medium though the port for inhalation (air sample inlet) and the reciprocating pump was restarted immediately so that the droplet would be dispersed quickly and mimic aspects of an inhaled therapy. On day 12, medium samples were collected and frozen for determination of urea and albumin. Then the devices were disassembled, the membrane and scaffolds were placed in 35 mm dishes and stained with Invitrogen live/dead stain (Invitrogen #L3224). Briefly, the Invitrogen live/dead stain was prepared by adding calcein-AM and ethidium homodimer-1 to Dulbecco's Phosphate Buffered Saline (DPBS) (final concentration of 2 μM for each fluorescent dye). The samples were stained for 30 min in the humidified incubator, at 5% CO_2 and 37°C. Then the samples were observed under a fluorescent microscope using FITC filter (494 nm excitation/517 nm emission) and RFP filters (528 nm excitation/617 nm emission). The live/dead stain discriminated live from dead cells simultaneously because the green-fluorescent calcein-AM indicates intracellular esterase activity (live) and red-fluorescent ethidium homodimer-1 indicates loss of plasma membrane integrity (dead). Figure 5A shows an example of the A549 lung cellular layer with the air-interface, HepG2 C3A cellular scaffold and MDA MB231 cellular scaffold after 48 hours in the lung device. We used ImageJ (National Institute of Health, Bethesda, Maryland) to determine viability based on areas of cells that picked up the fluorescent dyes.

Static Control Systems were assembled using the same pre-assembly procedures that were used for the devices but were conducted in 100 mm dishes. A rectangular silicone frame was cut with the VersaLaser so it would hold 1 mL total volume when pressed against a surface. This frame was autoclaved in a 100 mm glass petri dish on a Kimwipe, transferred into a new sterile 100 mm petri dish and pressed down so it would adhere to the bottom of that dish. On day 10, 1.0 mL of medium was placed in the silicone frame, pre-prepared HepG2 C3A and MDA MB231 cellular scaffolds were placed in that medium together, and then the pre-prepared lung membrane with air-interface was gently layered on top of this silicone frame preventing bubbles underneath the lung layer (the cells were exposed to the medium below and the humidified atmosphere from the incubator above). The 100 mm petri dish lid covered the assembly and was placed in the humidified incubator (5% CO_2 at 37°C) for 24 hours. After 24 hours (day 11), medium samples were collected for urea and albumin and frozen, medium replenished (50% replacement), static controls were split into groups (see above), 10 μL curcumin (0.25 mM or 2.5 mM) or medium was added on top of the lung cells or in the medium reservoir (below), and placed back in the humidified incubator. On day 12, medium samples were collected for urea and albumin, static controls were disassembled, the membranes and scaffolds were placed in 35 mm dishes and stained with Invitrogen live/dead stain (Invitrogen #L3224) and observed under an Olympus fluorescent microscope (Waltham, MA, #BX51WIF). We used ImageJ to determine viability based on areas of cells that picked up the fluorescent dyes. Figure 5A show fluorescent micrographs of each cell line (A549, HepG2 C3A, and MDA MB231) after 48 hours in the microfluidic device.

Urea and Albumin Synthesis

The cell culture medium was collected and frozen at −80°C after 24 h exposure in each device and each static control. Urea concentrations were measured using a DIUR assay kit

(BioAssay Systems #DIUR-500, Hayward, CA). We transferred 50 μL of the samples into the wells of a 96 well plate, added 200 μL chromogenic reagent (creates a stable colored complex that is urea specific), incubated for 20 min at room temperature and measured the optical density at 520 nm using a $VERSA_{max}$ microplate reader (Molecular Devices, San Jose, CA). The raw data was compared to a standard curve and expressed as mg/dL.

Albumin synthesis was evaluated by an Albumin Enzyme-Linked Immunosorbent Assay (ELISA) and following the manufacturer's directions. (Bethyl Laboratories #E80–129, Montgomery, TX). Briefly, we pre-coated the wells of a 96 well plate with goat anti-human albumin antibody, washed the wells with buffer and blocked with blocking buffer in the refrigerator overnight. We transferred 100 μL of the samples (diluted 1:50 sample diluent) into the coated wells. After incubating for 1 h at room temperature, we added HRP-conjugated goat anti-human antibody (1:75,000 dilution) to the wells and incubated again for 1 h. Following washing steps with buffer, we added 100 μL of enzyme substrate (tetramethylbenzidine) and incubated in the dark for 15 min. After adding stop solution, we measured the absorbance using the microplate reader at 450 nm. Data was compared to a standard curve and expressed as mg/mL.

Statistical Analysis

Data represent means of the experiments $\pm$ standard errors. The means were compared to each other using a two tailed Student t –test. A p-value of <0.05 was considered to be significantly different.

Immunostaining

After the air-interface was established, the A549 cells were fixed for 10 min in 4% paraformaldehyde at room temperature. The cells were washed with PBS plus 5% FBS, permeabilized with 0.25% Triton X-100 in PBS for 10 min at room temperature, and blocked with PBS containing 5% of bovine serum albumin (BSA) for 60 min at room temperature. The cells were labeled with ZO-1/TJP1 monoclonal antibody with FITC conjugate (ThermoFisher, Waltham, MA, #33–9111) diluted to 1 μg/mL in PBS containing 5% BSA, 1 h incubation. Finally the cells were washed with PBS and mounted with Fluorshield mounting medium with DAPI (Sigma #F6057) to stain the nuclei. Fluorescence was observed using the Olympus Fluorescent microscope (Figure 3B).

Results

Toxicity Experiments

Preliminary static toxicity experiments were done using MDA MB231 ($n = 3$) to compare our curcumin results with those previously published (Heger et al., 2014). We determined the in vitro LC_{50} concentration of curcumin to be 22 μM and 15 μM for a 24 hour exposure and 72 hour exposure, respectively. According to the Heger's review, our values were comparable to the reported static controls (Heger et al., 2014). Figure 4 compares the toxicity of curcumin on the MDA MB231 cells when exposed to various concentrations of curcumin after a 24 hour exposure and a 72 hour exposure.

We then determined if the delivery method (via reservoir (intravenous) vs. via lung (inhalation)) could affect toxicity of 2.5 μM and 25 μM curcumin on MDA MB231 in the microfluidic bidirectional lung device and static lung device. In the microfluidic lung device, there were significant decreases in the number of viable MDA MB231 cells of the curcumin treated groups when compared to the control ($p < 0.05$) using a two tailed Student t-test. It was also observed that there was a greater decrease in the number of viable MDA MB231 cells in 25 μM inhalation groups when compared to the 25 μM intravenous groups ($p < 0.05$) using a two tailed Student t-test. The A549 cells of the treated groups were not significantly different from each other or the A549 control ($p<0.05$). The liver cells of the 2.5 μM group showed a significant difference ($p < 0.05$), using a two tailed Student t-test, when compared to its control. However, the other liver cells of the other groups were not significantly different from their controls (Figure 5B). The difference in response maybe explained by the fact that standard error in the 2.5 μM inhaled group was small (SE = 0.97).

There was no significant differences in the viability of the MDA MB231 or the HepG2 C3A cells from their controls in the Static Device. There were significant differences observed in viability of A549 cells of the 2.5 μM intravenous and 25 μM inhalation treatment groups from their controls ($p < 0.05$) using a two tailed Student t-test (Figure 5C). Standard errors were calculated and included in these Figures. These results demonstrate that flow and recirculation of medium can be important when using multiorgan devices because the organ to organ interactions are limited under static conditions and dependent on diffusion.

We measured urea and albumin in the microfluidic lung device and static device before treatment and 24 hours after treatment with curcumin. There were no significant differences in the day 1 urea concentrations in the lung devices or the static devices. On day 2, we observed significant differences in all the curcumin treated groups when compared to the control microfluidic lung devices. The inhalation groups were significantly higher than the controls ($p < 0.05$) and the intravenous groups were significantly lower than the controls ($p < 0.05$) using a two tailed Student t-test (Figure 6A). Standard errors were calculated and included in this figure. This implies that curcumin has an effect on urea production and the means of exposure may also have an effect on the urea production.

The average values of albumin production in the microfluidic lung devices were not significantly different from the static devices, ranged from 2.46 to 2.74 mg/mL (Figure 6B). Standard errors were calculated and included in this figure. This implies that albumin production in the microfluidic device was not effected by curcumin.

Discussion

Effective therapy depends upon the drug delivery method (e.g. oral, intravenous administration, inhalation). When initially screening drugs for therapy the route of delivery must be considered (Labiris et al., 2003). The ability to model and test the different ways of drug administration could determine the most effective means of drug delivery for a patient. The results obtained in this study suggest that gravity-driven recirculating breathable lung device can be used to screen drugs that are being considered for inhalation and/or intravenous therapy for systemic or lung diseases. There are several advantages of our

pumpless system. Bidirectional flow uses a rocker platform for recirculation so drug absorption to external tubing, which maybe a confounding factor, is absent. The channel widths and heights are created to obtain desired fluid flow rates. The complete lung chamber incorporates an air-liquid interface and a breathable component which uses a reciprocating syringe pump for gas flow to simulated gas exchange, contraction and expansion of the lung chamber. Such a “breathable” component is more physiological than static systems and is incorporated here in a multiorgan device that contains a liver compartment and a tumor compartment. Hepatocytes and breast tumor cells are used to assess other organ and tumor toxicity. Also, these devices are easy to assemble and multiple units can be run at the same time, providing a low-cost means for screening drugs that are being considered for inhalation and/or intravenous therapy.

Specifically, the inhalation therapy feature of this microfluidic device introduces drug directly to the lung cells with the air-liquid interface and the breathable component before the drug enters the general circulation. The intravenous therapy feature introduces drug in the medium reservoirs of our lung devices where it is initially mixed and then distributes the drug into the circulation before exposing the compartments (organ) to the drug.

We determined that inhalation therapy could be more effective than intravenous therapy and an acceptable method to treat a patient with systemic disease. There were significant decreases in the viability of breast tumor cells of curcumin treated microfluidic groups when compared to the non-treated microfluidic groups. There was a greater decrease of viable MDA MB231 cells in the 25 μM inhalation therapy group when compared to the 25 μM intravenous therapy group after a 24 hour exposure confirming that the inhaled therapy was more effective than the intravenous therapy in the microfluidic device. The breathable portion of our device could be a contributing factor to this result. The mechanical effect of the expanding/contracting the membrane would cause a stretching/relaxing of the cells that could cause a physical effect and biological response. We note that the expansion of the membrane would increase air flow into the system providing more oxygen to the cells, and possibly supporting increased production of ATP providing energy or releasing phosphate groups for improved cellular metabolism and enhancing active transport of molecules into the system. The squamous type cells are responsible for the diffusion of water and electrolytes across the alveoli and the type II pulmonary epithelial cells have been used for drug metabolism. According to Foster et al., the A549 cell line may be useful for the studying the metabolic and macromolecule processing contributions of alveolar Type II cells to mechanisms of drug delivery at the pulmonary epithelium (Foster et al., 1998). Another factor to consider is the contracting or motion of the membrane itself during each cycle could also stimulate an increase in the release of waste or toxins, based on normal physiology (OpenStax College, 2013) or could just be enhancing the transport of the drug to the tumor chamber. Overall, the lungs of an organism provide a large vascular area of quick absorption and the possibility of enhanced active transport of a given drug could be appealing for many types of therapies. These results implied that inhalation therapy could be used as a possible therapy for systemic disease and ultimately making therapy easier for a patient by enabling home administration of pharmaceuticals.

Three improvements could be applied to increase the potential accuracy of our device. First, our reciprocating pump was capable of producing a fixed rate of 5 complete cycles/minute. The respiratory rate of a healthy adult male (12 and 18 breaths per minute) is larger and the use of a pump capable of 12 complete cycles would be desirable. Nonetheless, the results with our reciprocating pump suggest that inhalation therapy has promise and could be more effective than intravenous therapy. The second improvement would be to use cellular constructs that are more authentic than the cell lines used here. However, the basic device design would remain the same and using more authentic constructs should be easy. Third, the inhalation drug delivery could be improved by using a modified nebulizer unit to administrate the drugs to the lung. However by starting the reciprocating pump immediately after the addition of the drug we are providing drug distribution and mimicking inhalation delivery.

The toxicity of curcumin on MDA MB231 in the static device showed no significant differences when compared to the static controls however, there was a toxic effect in the static devices observed in lung cell viability for 2.5 μM administered into the reservoir and 25 μM administered into the lung chamber. These observations differed from those observed in the circulating devices showing that variability can exist in static devices and the lack of circulation can have an effect on certain cells in adverse ways.

Urea and albumin were measured before treatment and 24 hours after treatment with curcumin in the microfluidic lung device and static device. 24 hours after treatment, we observed significant differences in all the curcumin treated groups of the microfluidic lung devices when compared to the controls. The inhalation microfluidic groups were significantly higher than the controls and the intravenous microfluidic groups were significantly lower than the controls. The elevated levels of urea of the inhalation group could be caused by an elevated rate of metabolism of the liver type cells possibly stimulated by the inhalation therapy of curcumin. The lower levels of intravenous groups suggests that this route of exposure may also effect urea production. The static devices did not show any significant change in urea before or after curcumin treatment implying that circulation could be important.

The albumin production in the microfluidic lung devices groups were not significantly different when compared to those of the static devices. This implies that albumin production was not effected by curcumin or by circulation.

Our novel multi-organ bidirectional breathable lung with an air-interface device creates a means for comparing different routes of administrating drugs. Investigators have direct access to the air-interface of the breathable lung layer (model for inhalation) and access to medium reservoirs enabling drug mixing (intravenous model) before target cell exposure. This device can play a key role in determining if different modes of therapy are more beneficial or equivalent to each other. As an example, patients may be able to self-administer a chemotherapeutic drug at home by inhalation instead of having the added expense and inconvenience of a visit to the hospital or a physician’s office. A device such as described here could be an important step in determining when inhalation therapy maybe beneficial.

Acknowledgements

The authors would like to send a special thank you to Lincoln Young from INEng, LLC for designing and creating the reciprocating syringe pump for our research group. Also, a special thank you to Dr. Claudia Fischbach from Cornell University for the kind gift of MDA MB231 cells. This project was supported, in part, by the National Center for Advancing Translational Sciences at the National Institutes of Health (R44TR001326). Laser/Etch cutting of the lung devices were performed under the guidance of Beth Rhoades at the Cornell NanoScale Science and Technology Facility, a member of the National Nanotechnology Infrastructure Network, which is supported by the National Science Foundation (Grant ECS-0335765). Shuler is CEO of Hesperos, Inc. which builds and uses microphysiological systems for use by pharmaceutical firms to test potential drug candidates in human microphysiological systems, although this study is independent of Hesperos, Inc.

References

Benam KH, Villenave R, Lucchesi C, Varone A, Hubeau C, Lee HH, Alves SE, Salmon M, Ferrante TC, Weaver JC, Bahinski A, Hamilton GA, Ingber DE. (2016) Small airway-on-a-chip enables analysis of human lung inflammation and drug responses in vitro. Nat Methods, 13(2), 151–157. doi: 10.1038/nmeth.3697. [PubMed: 26689262]

Billington CK, Penn RB, Hall IP (2016) β2 Agonists. In: Page C, Barnes P (eds) Pharmacology and Therapeutics of Asthma and COPD Handbook of Experimental Pharmacology, 237, 23–40, Springer, Cham DOI 10.1007/164_2016_64

Douville NJ, Zamankhan P, Tung YC, Li R, Vaughan BL, Tai CF, White J, Christensen PJ, Grotberg JB, Takayama S. (2011) Combination of fluid and solid mechanical stresses contribute to cell death and detachment in a microfluidic alveolar model. Lab Chip, 11(4), 609–619. DOI: 10.1039/c0lc00251h [PubMed: 21152526]

Driscoll KE, Costa DL, Hatch GE, Henderson RF, Oberdorster G, Salem H, Schlesinger RB. (2000) Intratracheal instillation as an exposure technique for the evaluation of respiratory tract toxicity: Uses and limitations. Toxicological Sciences, 55(1), 24–35. [PubMed: 10788556]

Esch MB, King TL, Shuler ML. (2011) The role of body-on-a-chip devices in drug and toxicity studies. Annu Rev Biomed Eng, 13, 55–72. DOI: 10.1146/annurev-bioeng-071910-124629 [PubMed: 21513459]

Foster KA, Oster CG, Mayer MM, Avery ML, Audus KL. (1998) Characterization of the A549 cell line as a type II pulmonary epithelial cell model for drug metabolism. Exp Cell Res, 243 (2):359–66. DOI: 10.1006/excr.1998.4172. [PubMed: 9743595]

Foty R (2011) A simple hanging drop cell culture protocol for generation of 3D spheroids. J of Vis Exp, 51, 2720. doi: 10.3791/2720

Haber S, Clark A, Tawhai M. (2013) Blood flow in capillaries of the human lung. J Biomech Eng, 135(10), 101006–101011. doi: 10.1115/1.4025092. [PubMed: 23897065]

Heger M, van Golen RF, Broekgaarden M, Michel MC. (2014) The molecular basis for the pharmacokinetics and pharmacodynamics of curcumin and it metabolites in the relation to cancer. Pharm Reviews, 66, 222–307. doi: 10.1124/pr.110.004044.

Humayun M, Chow C-W, Young EWK. (2018) Microfluidic lung airway-on-a-chip with arrayable suspended gels for studying epithelial and smooth muscle cell interactions. Lab Chip, 18, 1298–1309. DOI: 10.1039/C7LC01357D [PubMed: 29651473]

Huh D (2015) A human breathing lung-on-a-chip. Ann Am Thorac Soc, 12(Suppl 1), S42–S44. 10.1513/AnnalsATS.201410-442MG [PubMed: 25830834]

Huh D, Leslie DC, Matthews BD, Fraser JP, Jurek S, Hamilton GA, Throneloe KS, McAlexander MA, Ingber DE. (2012) A human disease model of drug toxicity-induced pulmonary edema in a lung-on-a-chip microdevice. Sci Transl Med, 4(159), 159ra147. DOI: 10.1126/scitranslmed.3004249

Huh D, Matthews BD, Mammoto A, Montoya-Zavala M, Hsin HY, Ingber DE. (2010) Reconstituting organ-level lung functions on a chip. Science, 328 (5986), 1662–1668. DOI: 10.1126/science.1188302 [PubMed: 20576885]

Irvin CG, and Bates JHT. (2003) Measuring the Lung Function in the Mouse: The Challenge of Size. Respir Res, 4(1), 4. doi: 10.1186/rr199 [PubMed: 12783622]

Jain A, Barrile R, van der Meer AD, Mammoto A, Mammoto T, De Ceunynck K, Aisiku O, Otieno MA, Louden CS, Hamilton GA, Flaumenhaft R, Ingber DE. (2018) Primary human lung alveolus-on-a-chip model of intravascular thrombosis for assessment of therapeutics. Clin Pharmacol Ther, 103(2), 332–340. 10.1002/cpt.742 [PubMed: 28516446]

Konar D, Devarasetty M, Yildiz DV, Atala A Murphy SV. (2016) Lung-on-a-chip technologies for disease modeling and drug development. Biomed Eng Comput Biol, 7(Suppl 1), 17–27. doi: 10.4137/BECB.S34252 [PubMed: 27127414]

Labiris NR, and Dolovich MB. (2003) Pulmonary drug delivery. Part I: Physiological factors affecting therapeutic effectiveness of aerosolized medications. Br J Clin Pharm, 56(6), 588–599. doi: 10.1046/j.1365-2125.2003.01892.x

Long C, Finch C, Esch M, Anderson W, Shuler M, Hickman J. (2012) Design optimization of Liquid-phase flow patterns for microfabricated lung on a chip. Ann Biomed Eng, 40(6), 1255–1267. DOI: 10.1007/s10439-012-0513-8 [PubMed: 22271245]

Los Alamos NL PuLMo. (2016) Tiny plastic lung mimics human pulmonary function. http://www.lanl.gov/discover/news-release-archive/2016/April/04.25-human-pulmonary-function.php

Mak IWY, Evaniew N, Ghert M. (2014) Lost in translation: animal models and clinical trials in cancer treatment. Am J Transl Res, 6(2), 114–118. www.ajtr.org/ISSN:1943-8141/AJTR1312010 [PubMed: 24489990]

Miller PG, Shuler ML. (2016) Design and demonstration of a pumpless 14 compartment microphysiological system. Biotech Bioeng, 113(10), 2213–2227. DOI 10.1002/bit.25989

Morier P, Vollet C, Michel PE, Reymond F, Rossier JS. (2004) Gravity-induced convective flow in microfluidic systems: Electrochemical characterization and application to enzyme-linked immunosorbent assay tests. Electrophoresis, 25, 3761–3768. 10.1002/elps.200406093 [PubMed: 15565685]

Nalayanda DD, Puleo C, Fulton WB, Sharpe LM, Wang TH, Abdullah F. (2009) An open-access microfluidic model for lung-specific functional studies at an air-liquid interface. Biomed Microdevices, 11(5), 1081–1089. DOI: 10.1007/s10544-009-9325-5 [PubMed: 19484389]

Nikolic MZ, Rawlins EL. (2017) Lung organoids and their use to study cell-cell interaction. Curr Pathobiol Rep, 5, 233–231. DOI 10.1007/s40139-017-0137-7 [PubMed: 29270332]

OpenStax College (2013) Anatomy and Physiology. OpenStax CNX http://cnx.org/contents/14fb4ad7-39a1-4eee-ab6e-3ef2482e3e22@11.1.

Persson CG. (2002) Con: mice are not a good model of human airway disease. Am J Resp Crit Care Med, 166(1), 6–8. 10.1164/rccm.2204001 [PubMed: 12091161]

Pezzulo AA, Starner TD, Scheetz TE, Traver GL, Tilley AE, Harvey BG, Crystal RG, McCray PB Jr., Zabner J (2011) The air-liquid interface and use of primary cell cultures are important to recapitulate the transcriptional profile of in vivo airway epithelia. Am J Physiol Lung Cell Mol Physiol, 300(1), L25–L31. doi: 10.1152/ajplung.00256.2010 [PubMed: 20971803]

Potkay JA, Magnetta M, Vinson A, Cmolik B. (2011) Bio-inspired, efficient, artificial lung employing air as the ventilating gas. Lab on a Chip, 11(17), 2901–2909. DOI:10.1039/c1lc20020h [PubMed: 21755093]

Price PS, Conolly RB, Chaisson DF, Gross EA, Young JS, Mathis ET, Tedder DR. (2003) Modeling interindividual variation in physiological factors used in PBPK models of humans. Crit Rev Toxicol, 33(5),469–503. 10.1080/10408440390242324 [PubMed: 14594104]

Ragohna EW, Martinaz EF, Muzilli CA, Miranda ME, Novaes Olivieri KA. (2015) Cytotoxicity analysis of electrostatically applied epoxy coating onto CO-CR alloy. RGO, Rev Gaúch Odontol, Porto Alegre, 63(3), 257–262. 10.1590/1981-86372015000300012838

Stucki JD, Hobi N, Galimov A, Stucki AO, Schneider-Daum N, Lehr C-M, Huwer H, Frick M, Funke-Chambour M, Geiser T, Guenat OT. (2018) Medium throughput breathing human primary cell alveolus-on-chip model. Sci Rep, 8, 14359. DOI: 10.1038/s41598-018-32523-x

Stucki AO, Stucki JD, Hall SRR, Felder M, Mermoud Y, Schmid RA, Geiser T, Guenat OT. (2015) A lung-on-a-chip array with an integrated bio-inspired respiration mechanism. Lab Chip, 15, 1302–1310. DOI: 10.1039/C4LC01252F [PubMed: 25521475]

Sung JH, Kam C, Shuler ML. (2010) A microfluidic device for a pharmacokinetic-pharmacodynamic (PK-PD) model on a chip. Lab Chip, 10(4), 446–455. DOI: 10.1039/b917763a [PubMed: 20126684]

Tu Y-P, Larsen GL, Irvin CG. (1995) Utility of murine systems to study asthma pathogenesis. Eur Respir Rev, 29, 224–230.

Wang YI, Carmona C, Hickman J, Shuler ML. (2018) Multiorgan microphysiological systems for drug development: strategies, advances, and challenges. Adv Healthcare Mat, 7(2), 1701000. 10.1002/adhm.201701000

Wang YI, Oleaga C, Long CJ, Esch MB, McAleer CW, Miller PG, Hickman J, Shuler ML. (2017) Self-contained, low-cost body-on-a-chip systems for drug development. Exp Bio Med, 242(17), 1701–1713. 10.1177/1535370217694101

Zaidi D, Singh N, Ahmad IZ, Sharma R, Balapure AK. (2011) Antiproliferative effects of curcumin plus centchroman in MCF-7 and MDA MB-231 cells. Internat J of Pharm and Pharm Sci, 3(2), 212–216.

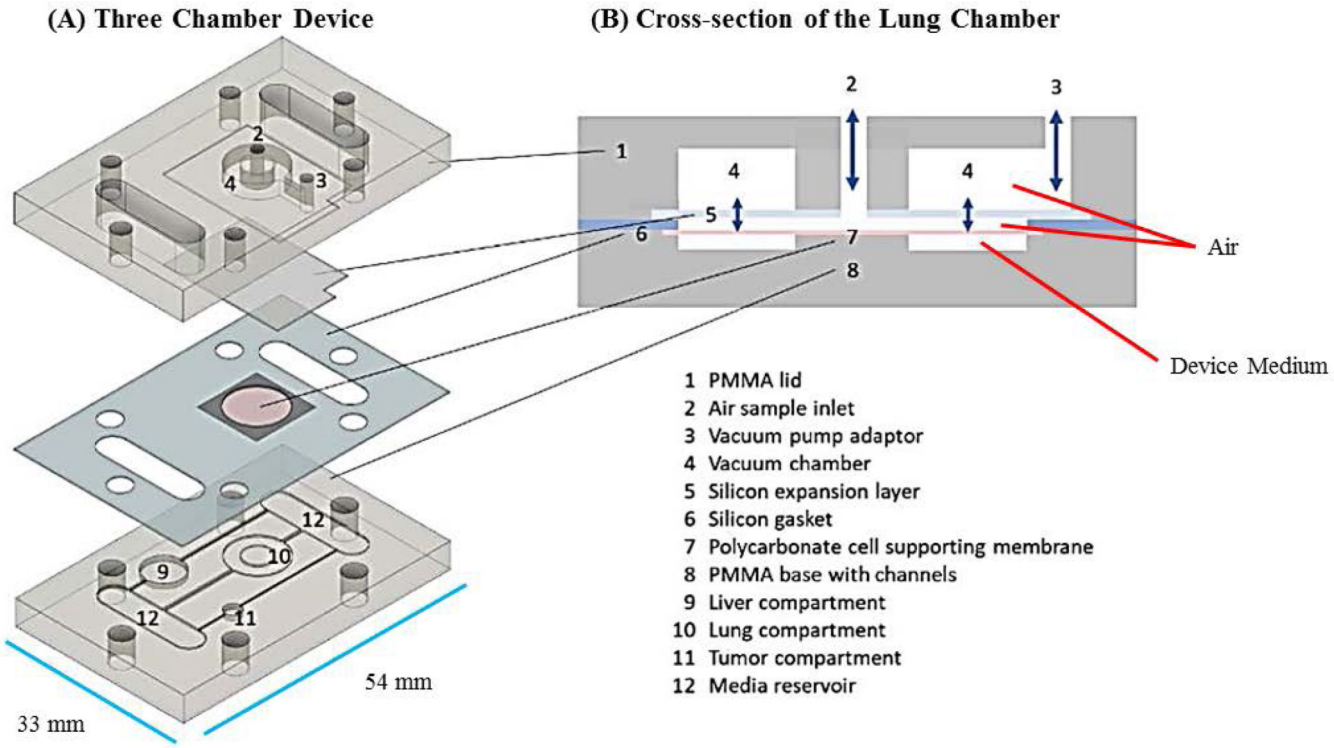

(C)

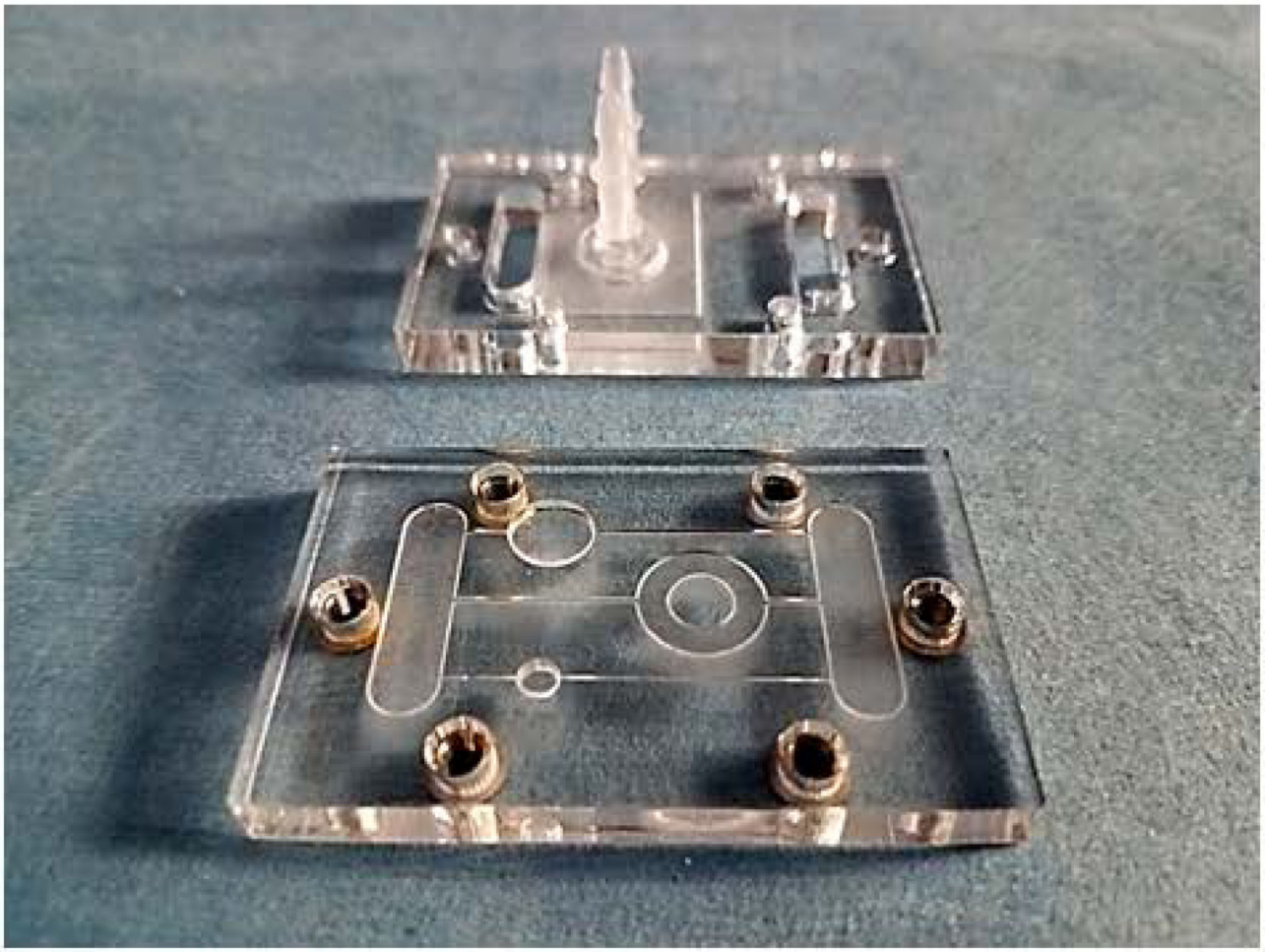

(D)

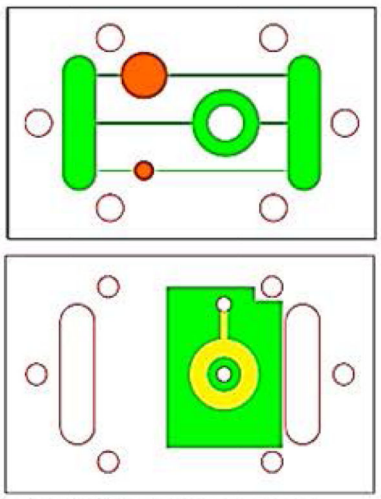

Gasket (0.5 mm Silicone sheet):

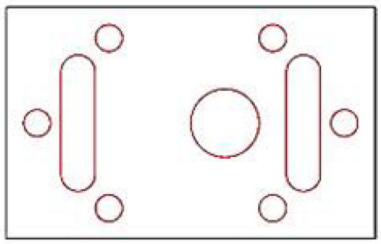

Expansion layer (0.25 mm Silicone sheet):

Bottom and top frames of the lung device

Order	Color	Power, %	Speed, %	PPI	Z-axis	Mode
1-1	Orange	25	20	1000	5.5	Raster
1-2	Green	11.2	20	1000	5.5	Raster
1-3	Red	100	2.2	1000	5.5	Vector
1-4	Black	100	2.2	1000	5.5	Vector

Order	Color	Power, %	Speed, %	PPI	Z-axis	Mode
1-1	Yellow	35	20	1000	5.5	Raster
2-1	Yellow	35	20	1000	5.0	Raster
2-2	Green	17	20	1000	5.5	Raster
2-3	Red	100	2.2	1000	5.5	Vector
2-4	Black	100	2.2	1000	5.5	Vector

Silicone Layers that make up the lung layer

Order	Color	Power, %	Speed, %	PPI	Z-axis	Mode
1-1	Red	15	10	1000	0.5	Vector
1-2	Black	15	10	1000	0.5	Vector

Silicone expansion layer

Order	Color	Power, %	Speed, %	PPI	Z-axis	Mode
1-1	Red	15	10	1000	0.5	Vector
1-2	Black	15	10	1000	0.5	Vector

Figure 1.

Schematic of a multi-organ microfluidic platform with a breathable lung chamber. (A) A 3-chamber microfluidic device that has (a) an accessible lung compartment with a breathable component produced using a reciprocating syringe pump connected to a vacuum chamber (complete lung chamber), (b) a liver compartment and (c) a tumor compartment. The device consists of polymethyl methacrylate housing (PMMA), polycarbonate (PC) membrane and silicone gaskets. The device is held together with small stainless steel screws. The compartments and reservoirs are connected by individual channels for culture medium distribution. (B) Cross-section of the lung chamber. The complete lung chamber consisted of an inlet (for inhalation therapy), a vacuum chamber, an air component, a cellular layer on a membrane, and a medium compartment. (C) Actual photographs of the frame (PMMA lid and base) of the microfluidic platform with a breathable lung chamber. The device was maintained on a programmable rocker platform to obtain gravity-driven bidirectional flow, Infinity Rocker Platform, 60 s with each side in the highest position, with a 1 s flip in

between and repeat. (D) Design and settings for the VersaLaser cutting and etching patterns of the silicone gaskets, PMMA lid and base for the multi-organ microfluidic platform.

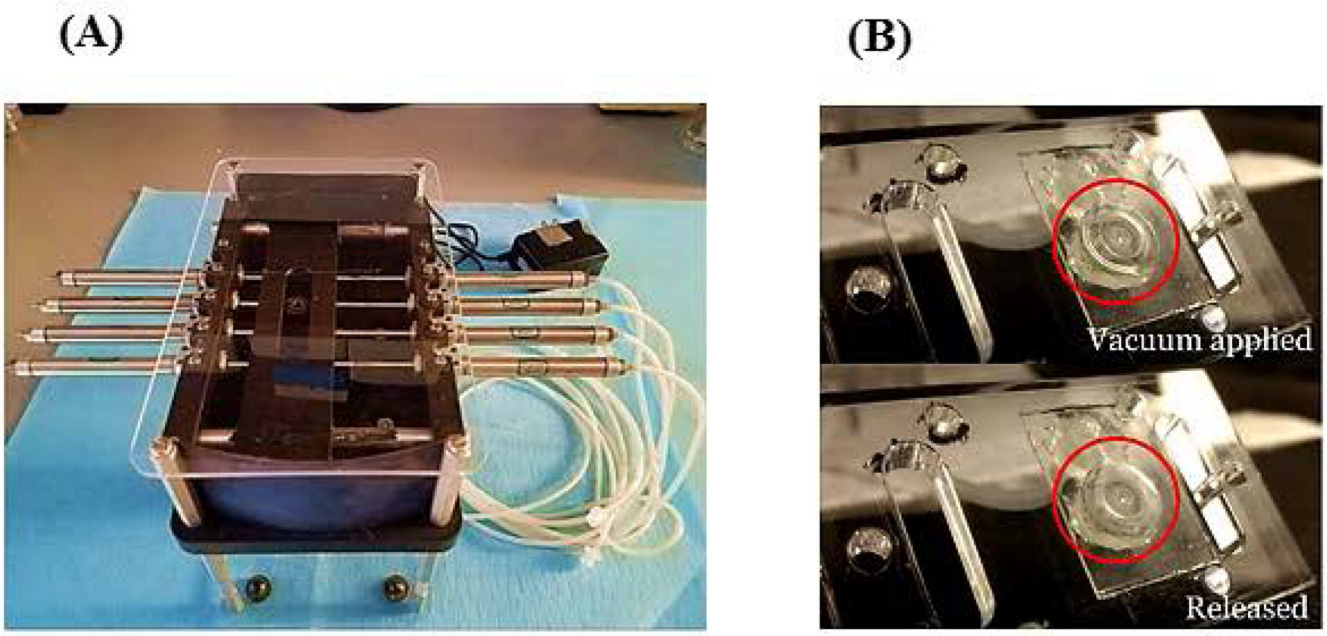

Figure 2.

Membrane expansion created using reciprocating syringe pump. (A) Photograph of the reciprocating syringe pump with tubing. The inlet of the vacuum chamber of the device was connected to a silicone tube with a 0.2 μ pore size filter (to maintain sterility), with another length of sterile silicone tubing and then to the vacuum pump. The membrane expansion was controlled through the pressure change driven by this reciprocating syringe pump and was key for the breathable component of the lung chamber. (B) Photograph of the expansion of the membrane during the time when the vacuum was applied and released. This demonstrated that the epoxy adhesion could be used to adhere the gasket to the frame and sustain the stretching of the gasket.

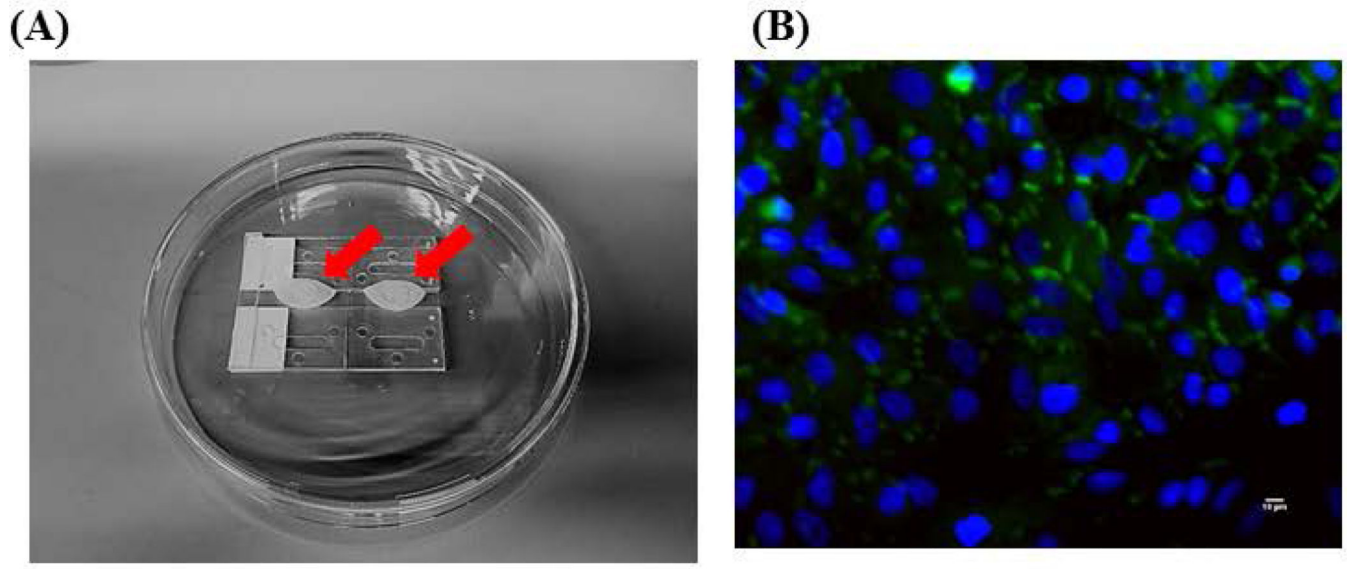

Figure 3.

Air-liquid interface Bridge and Immunostaining of A549 cells. (A) Two sets of 2 microscope slides (1” × 3”) were space 6 mm apart and adhered together using silicone sealant and 1 silicone strip (87 mm long × 5–6 mm wide × 1.6 mm thick). This was placed in a 150 mm petri dish and autoclaved. Two lung gasket membranes were placed on top of the bridge on Day 3. 20 mL of device medium was pipetted below the bridge, every other day 50% of the medium was exchanged until Day 10 (device assembly). A red arrow indicates where the lung cells (A549) were plated and how the air-liquid interface sits on top of the Bridge. (B) Fluorescent micrographs (400× magnification) of A549 cells on Day 10 were observed after immunostaining under a fluorescent microscope for tight junctions (protein ZO-1, green). The nuclei were counter-stained (DAPI, blue). Scale bars (10 μ) are present on the micrographs.

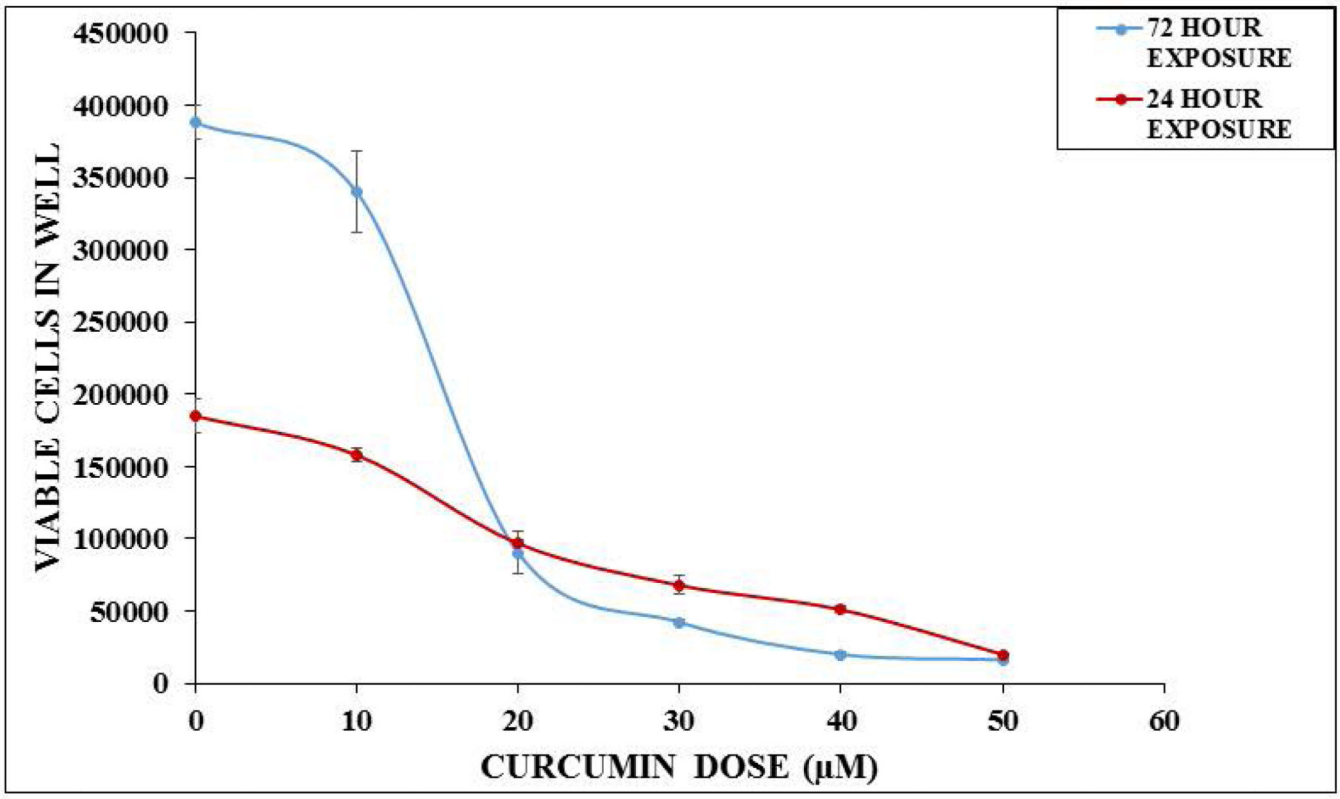

Figure 4.

In vitro static toxicity of curcumin on MDA MB231 (breast) cells. MDA MB231 cells were resuspended at 5×10^{-4} cells/mL, 1 mL of the suspension was plated into 6 well-plates. After 24 hours, the plates were divided into the following groups: (a) Control (b) 1 µM curcumin (c) 10 µM curcumin (d) 20 µM curcumin (e) 30 µM curcumin (f) 40 µM curcumin (g) 50 µM curcumin. Cell densities were determined using a hemocytometer after 24 hours or 72 hours of curcumin exposure. Data are expressed as standard error of the mean (n = 3 separate experiments). The *in vitro* LC50 values were calculated to be 22 µM and 15 µM, respectively.

(A)

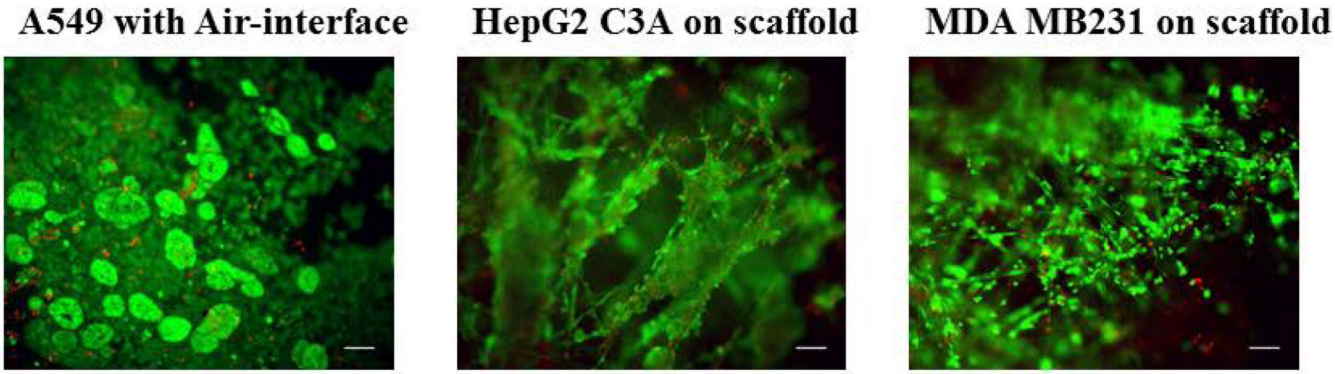

(B)

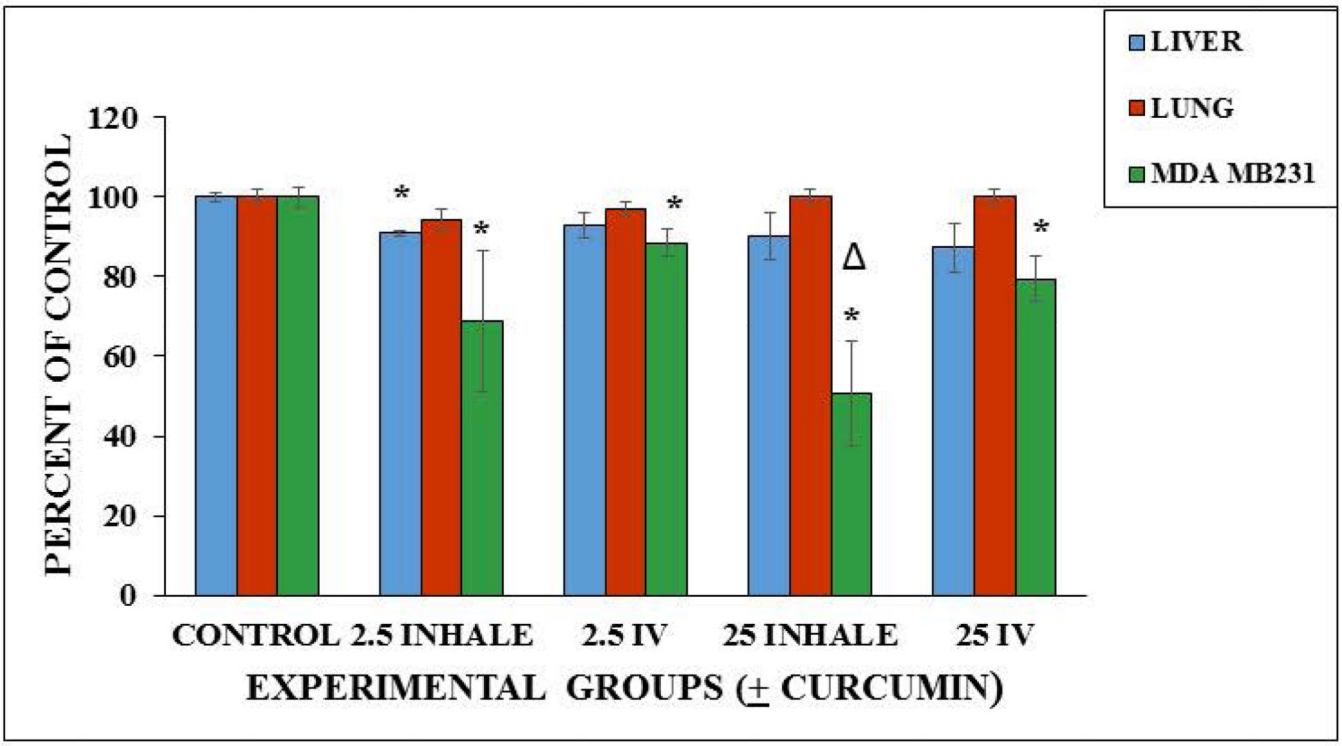

(C)

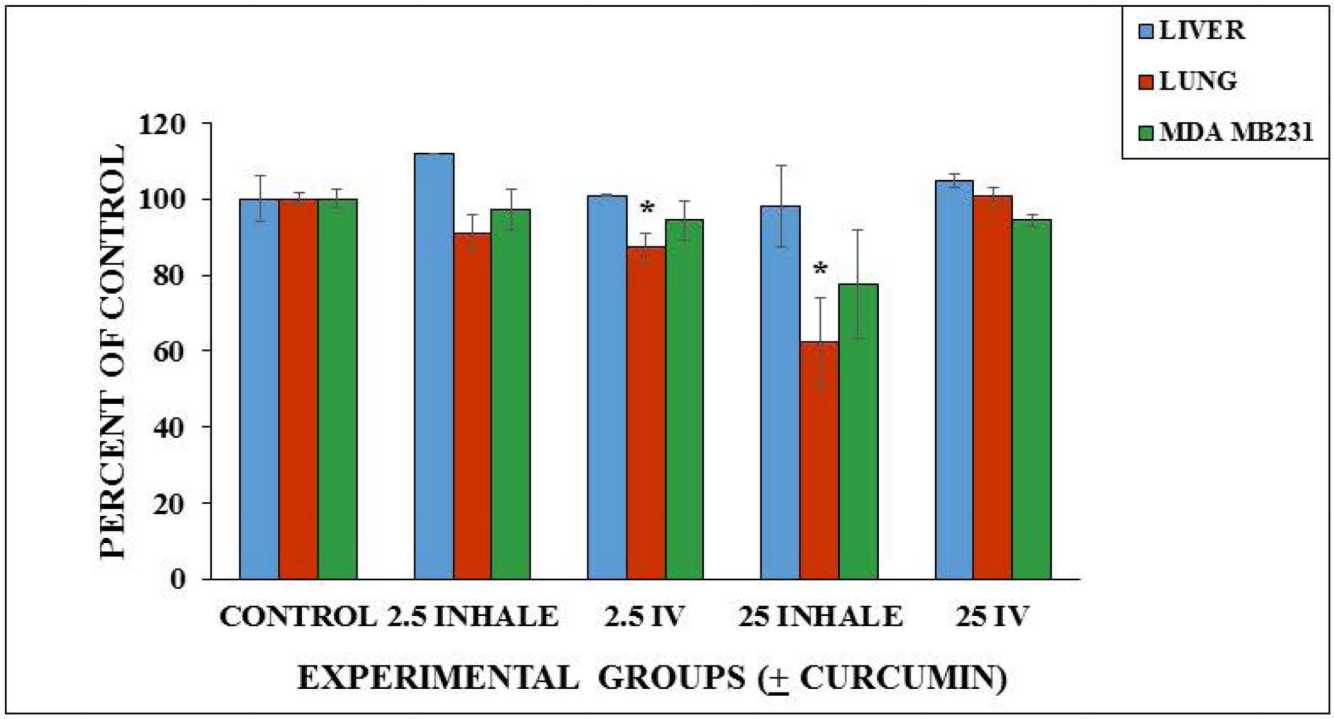

Figure 5.

Device viability after 48 hours and viability after 24 hour curcumin exposure. (A) Fluorescent micrographs (100× magnification) of 48 hour viability of the three cell lines (A549, HepG2 C3A, and MDA MB231) maintained in the lung device (using fluorescent Live/Dead Stain). Scale bars (100 μ) are present on the micrographs. (B) Viability in the microfluidic lung device after 24 hour curcumin exposure. Values are shown as the average percent viable (n = 3). Values are means ± SEM. Significant differences ($p < 0.05$) using a two tailed student t-test between the controls and curcumin exposed groups are indicated with an asterisk (*). Significant difference ($p < 0.05$) between the 25 μM intravenous group and the 25 μM inhaled group is indicated with a triangle (Δ). (C) Viability in the static device after 24 hour curcumin exposure. Values are shown as the average percent viable (n = 3). Values are means ± SEM. Significant differences ($p < 0.05$) using a two tailed student t-test between the controls and curcumin exposed groups are indicated with an asterisk (*).

(A)

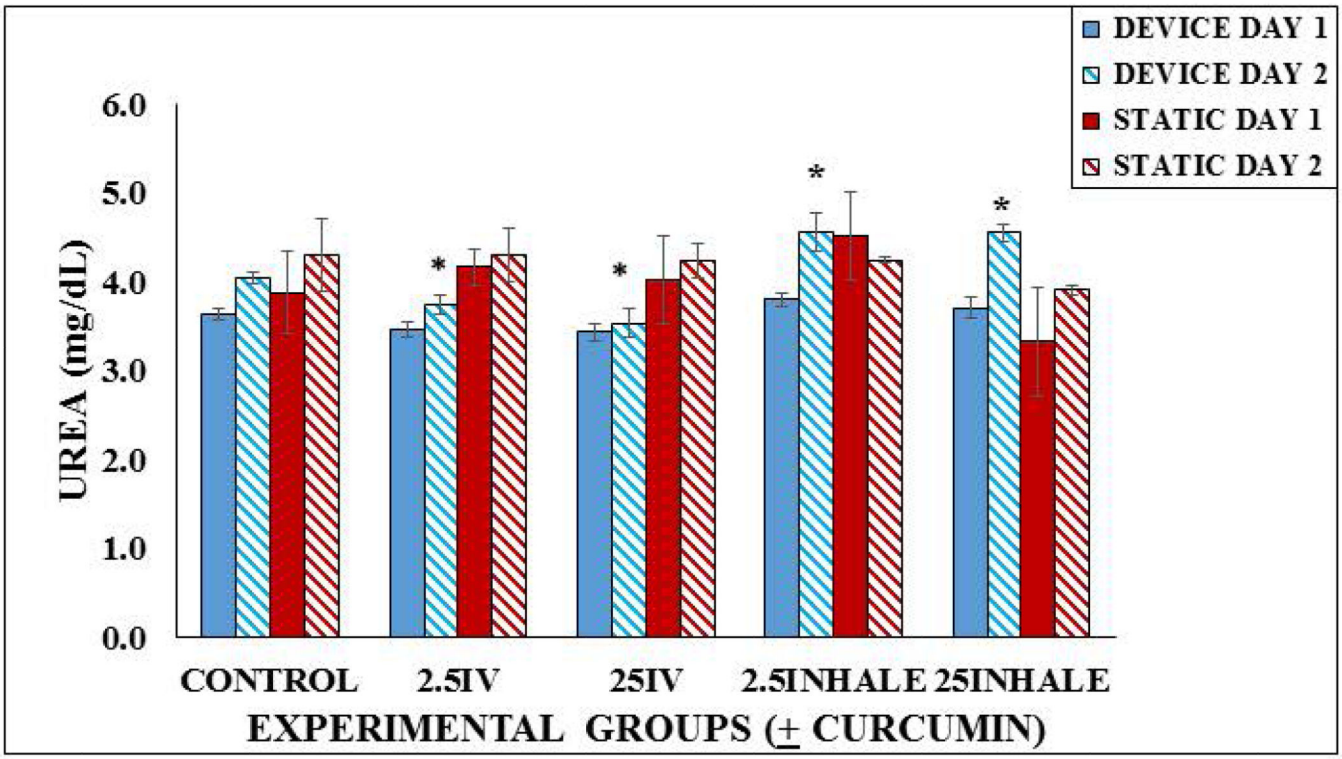

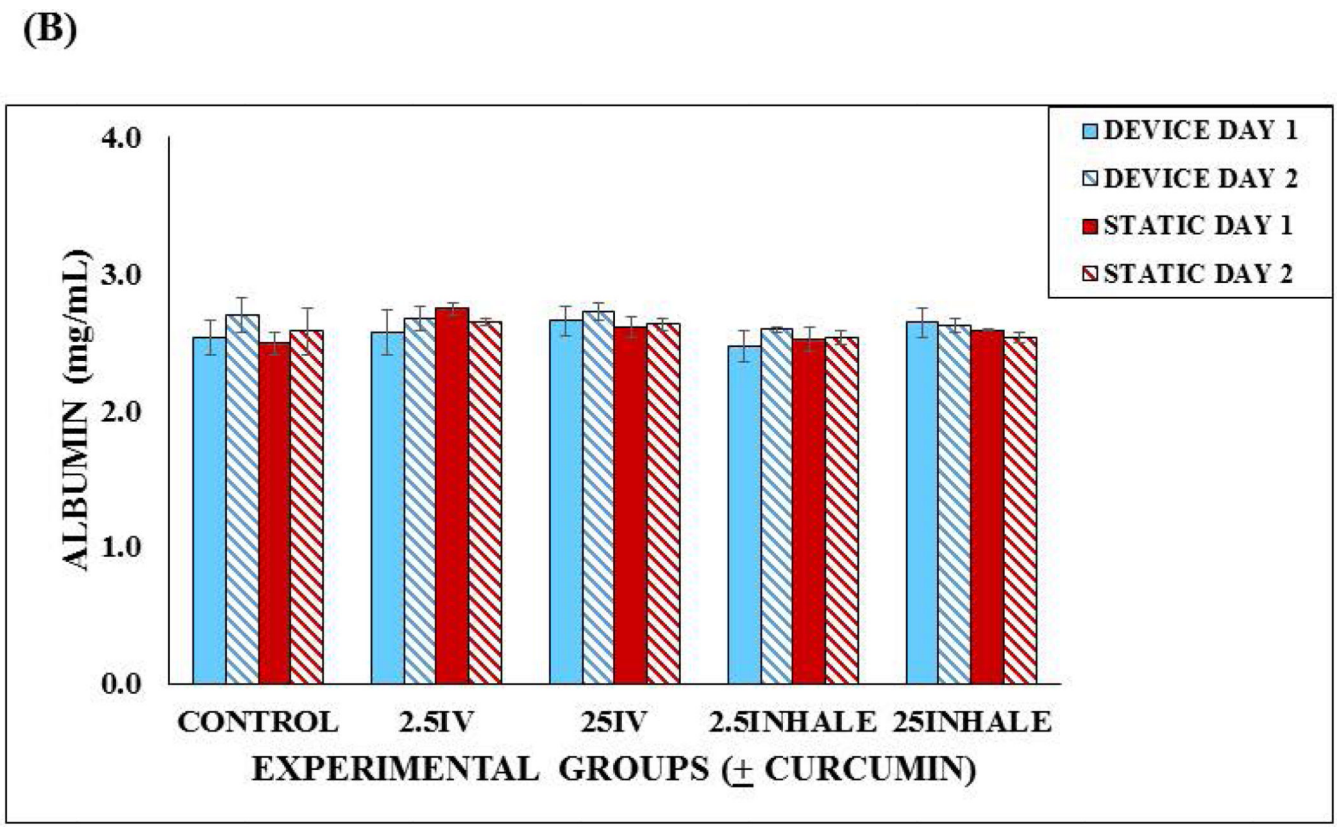

Figure 6.

Functionality of the microfluidic lung device versus the static device. (A) Urea production in the Lung Device vs. Static Control over a 48 hours. Samples were taken after a 24 hour incubation and then after a 24 hour exposure with fresh device medium, 2.5 μM or 25 μM curcumin into reservoir (intravenous (IV)) or via lung chamber (inhaled). Each sample was run in duplicate and 3 separate experiments were completed (n = 3). Values are means ± SEM. Significant differences ($p < 0.05$) using a two tailed student t-test between the controls and curcumin exposed groups are indicated with an asterisk (*). (B) Albumin production in the Lung Device vs. Static Control over a 48 hours. Samples were taken after a 24 hour incubation and then after a 24 hour exposure with fresh Device Medium, 2.5 μM or 25 μM curcumin into reservoir (intravenous (IV)) or via lung chamber (inhaled). Each sample was run in duplicate and 3 separate experiments were completed (n = 3). Values are means ± SEM. No significant differences were observed.

Table 1.

Physiological information, calculations used to create the lung device. Physiological human male organ volumes and flow rates from the literature (Haber et al., 2003; Price et al., 2000) were scaled down to create our device's organ volumes and residence times. Residence time = organ volume/flow rate. The channel dimensions were estimated by using the Hagen–Poiseuille's equation, the channel's cross-sectional areas, volumetric flow rates (desired) and linear flow rates (desired) were calculated for the device held at a 5 degree angle.

Organs	Organ volumes from literature (liters)	Device organ volumes (μL)	Flow rate from literature (L/min)	Residence time (min)	Channel X-sectional area (mm^2)	Calculated flow rate (Desired) (μL/s)	Calculated linear flow rate (Desired) (mm/s)
Lung	1.01	30.3	2.44	0.41	0.152	1.22	8.0
Liver	1.57	47.1	1.32	1.19	0.116	0.66	5.7
Tumor	0.10	3.0	0.06	1.67	0.028	0.03	1.1